Roll to Roll Imprinting PDMS Microstructures Under Reduced Ambient Pressures

Olli-Heikki Huttunen, Johanna Hiitola-Keinänen, Jarno Petäjä, Eero Hietala, Hannu Lindström, and Jussi Hiltunen

***Abstract*— High-volume manufacturing of microstructures is essential for the uptake of the related scientific results for commercial use and also if hundreds or thousands of devices with repeatable performance are needed during the large-scale experimental research. Polydimethyl siloxane (PDMS) is one of the most widely used materials for academia to prepare microfluidic test devices. This has also motivated the development of roll-to-roll imprinting towards the fabrication of PDMS-based devices at high volumes. The gas bubble entrapping during the replication process has remained an issue resulting in defects in the microstructure. Performing imprinting in vacuum is a well-known method to avoid bubbles but it has not been applied in roll-to-roll processing. In this work we demonstrated a reduced ambient pressure roll to roll imprinting process using PDMS silicone elastomer as imprint resist. We observed the reduction in the number of bubble-originated defects in individual micro-features from 100 % to < 1 % when the ambient pressure was reduced from 1 atm to 1/8 atm. [2023-0063]**

***Index Terms*— Elastomer, imprinting, manufacturing processes, micromechanical systems, nanoimprint lithography, PDMS, production manufacturing, R2R, replication, roll-to-roll, silicone, vacuum technology.**

I. Introduction

FOR two decades room temperature vulcanizing (RTV) silicone elastomers, commonly called by their chemical backbone, polydimethylsiloxanes (PDMS), has been a common group of materials for prototyping micromechanics and especially microfluidics. PDMS-based prototypes are typical in biomedical applications enabling different electronic, optical, and micromechanical functions. [1], [2], [3], [4], [5] PDMS provides many favorable features, such as the possibility for easy micromolding and bonding [6] together with biocompatibility [7]. All of these properties enable the usage of silicones even in implants/prosthetics. Organ-on-chip is another rapidly growing research topic where PDMS replication is used [8]. Furthermore, artificial organs are developed [9]

Manuscript received 13 April 2023; revised 27 September 2023; accepted 7 November 2023. Date of publication 5 December 2023; date of current version 5 February 2024. This work was supported in part of the Finnish Academy "Printed Intelligence Infrastructure" under Grant 32002 and in part by the Horizon 2020 Project MedPhab under Grant 871345. Subject Editor R. Sochol. *(Corresponding author: Olli-Heikki Huttunen.)*

The authors are with the VTT Technical Research Centre of Finland, 90570 Oulu, Finland (e-mail: Olli-Heikki.Huttunen@vtt.fi).

This article has supplementary material provided by the authors and color versions of one or more figures in this article are available at https://doi.org/10.1109/JMEMS.2023.3336740.

Digital Object Identifier 10.1109/JMEMS.2023.3336740

There are two high-volume manufacturing methods that can be used with liquid silicone rubbers (LSR) to produce micromolded parts. These include injection molding [10] and another high precision fabrication method called imprinting, or nanoimprinting, in which a master template is applied as a mold for replication of surface reliefs into curable polymer [11]. Imprinting is used as production method for various of products with most notably in light guiding applications [12]. High throughput production can be done with a sheet-based process or high-volume roll-to-roll (R2R) process [13], [14]. Still less than a decade ago, RTV PDMS materials were considered suitable only for prototyping purposes in the field of micromolding [15]. Recently, mass production methods such as roll to roll) replication of PDMS have been demonstrated for the realization of microstructures [16] and nanostructures [14], [16]. As several different functionalities can be implemented by R2R techniques on silicone substrates, [17], [18] it is ultimately possible to fabricate integrated systems comprising several PDMS-based components. One roll-to-roll (R2R) and large-area-compatible coating method for PDMS is knife coating [19]. This knife coating process also enables the possibility to introduce patterns into the film during film fabrication [20]. Besides enabling the industrial scale fabrication of disposable, or other low-cost devices, mass manufacturing techniques also allows the fabrication of large batches of devices with uniform quality for research purposes. These case types are, for example, pre-clinical studies where a large number of devices with a repeatable performance are needed to collect statistically relevant data. Previous numerical analyses have compared roll-based and sheet-based processes, expecting a relevant similarity in mold filling behavior [21].

Bubble formation is a common issue causing defect formation in imprinting processes. This is due to gas bubbles being entrapped inside the resist material during the coating phase due to stirring [22]. Alternately gas bubbles can be trapped when the mold comes into contact with the resist leaving a cavity type defect when the resist is cured [23], [24]. The issue can be tackled by adjusting basic process parameters:

- Effect of the web speed: this can be attributed to mold filling time [21]. Slower web speeds enable longer mold filling time and thus decrease amount and size of bubbles.
- Increased imprint pressure: observed to prevent bubble entrapping due to increased air dissolution rate [23].
- Material selection: which can affect to surface contact angle and fluid viscosity [25].

- Increased temperature: leads to decreased resist viscosity, which reduces the bubble formation [21], [23], [26]. However, elevated temperature also rapidly increases the viscosity of thermally cured resist when curing reaction takes place.

Another proposed method to reduce the amount of the entrapped gas bubbles, is to use helium atmosphere to increase the diffusion rate of bubbles in to imprint resist matrix. [26] Or to use condensable gas atmosphere to transform gas bubbles into liquid form and then dissolve in the imprint resist matrix [27], [28].

Furthermore, one option to avoid entrapped air bubbles is to perform the replication in a reduced gas environment, or vacuum, which in practice is more accurately a reduced ambient gas pressure [26]. Subsequently, even under partial vacuum bubbles may be generated onto the imprint resist. Adsorption of the gas in the resist material is one mechanism to get rid of the gas bubbles and it takes place also with air [28], [29]. Low ambient pressure decreases solubility of the gas to the imprint resist, whereas additional imprint pressure increases solubility [30]. Dissolution or diffusion of the gas bubble, however, takes time. In high throughput R2R process imprint resist may remain in liquid form only for seconds after mold filling at most and therefore dissolution can be seldom exploited

In this work, we demonstrated a R2R imprinting process at pressure levels of 100 kPa, 50 kPa, 25 kPa and 12.5 kPa, corresponding to 1, 1/2, 1/4 and 1/8 atmospheric pressure (atm), respectively. By investigating the effect of different ambient gas pressures on the amount of the air bubbles in the replicated rectangular pillar structures we were able to achieve bubble free imprint replication by modifying process parameters and component design. However, the critical parameters are case dependent and related to material use, structure, and other process parameters, which may set limitations for the design and choice of materials. Residual layer thickness is one such parameter which may be demanded. Significance of residual layer thickness was described in more detail by Yang et al. [31] PDMS devices typically require a significant residual layer thickness, making the imprint resist prone to stirring during the imprint infeed. According to a numerical study by Ye et al., stirring is one major factor that causes bubbles [22]. Overall, bubble formation and bubble entrapping is a complex phenomenon of multiple factors, and all those factors can seldom be controlled freely. To our knowledge there is no previous literature on implementation of a R2R imprinting process in vacuum or reduced ambient gas pressure. Including our previous work, there are only a few reports of roll imprinting of PDMS [16], [32]. However, we assume that the basic principles of the bubble entrapping mechanism are the same for both types of liquid resists (whether thermally curable or UV curable).

II. Microstructure Fabrication by R2R Imprinting Process

R2R replication was accomplished with a custom made, sealed R2R imprinting line manufactured by Norbert Schläfli AG. The model closest to our device in the manufacturer's range is the Explorer 750, which also partially serves as the basis for the customized machine. Customization involves in modified web path, gas-tight steel plating and sealed doors constructed from thick aluminum, equipped with heavy-duty windows. All seams and the electrical and pneumatic pass-throughs have been sealed. The imprint unit is also distinctive and has been custom-made (designed and implemented by MK Fluidics). Machine construction and imprint process is illustrated in **Fig. 1** as images (**Fig. 1a** and **Fig 1c**) (**and** as a drawing **Fig 1b**). Optical image of the machine is presented in Supplementary material (**S1**). As the machine is sealed entirely, creation of a partial vacuum within it is enabled. All winders, guiding rolls, idle rolls, and the imprint unit are located inside the machine.

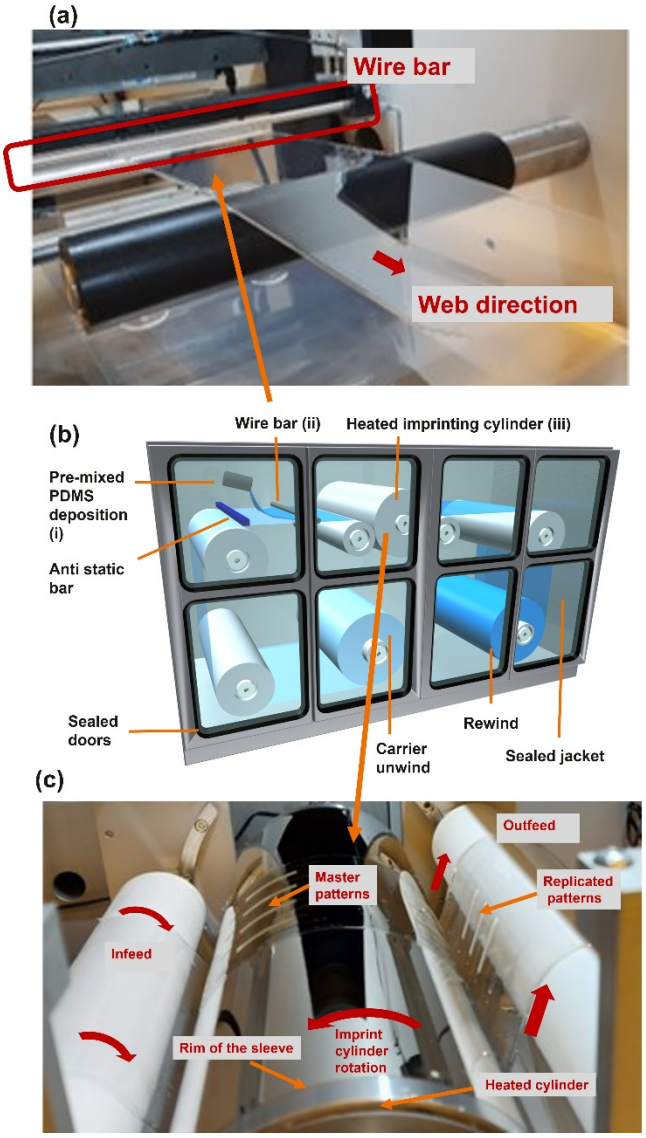

Fig. 1. (a) Wire bar levelling of deposited silicone. (b) 3D illustration of imprinting in sealed R2R machine. (c) Thermal cure R2R imprinting.

A. Tooling by Photolithography

The imprint mold was fabricated on a 0.15 mm thick electroformed nickel plate (100 × 100 mm) with negative-tone photoresist features (SU-8, purchased from micro resist technology GmbH). The mold consisted of two photoresist layers.

The first layer was a thin uniform layer covering the whole plate. The purpose of the first layer is to provide a smooth surface for the second patterned layer and to improve the adhesion between the mold microstructures and the supporting nickel plate. The nickel plate was first rinsed with acetone and isopropanol. The excess isopropanol was removed with a nitrogen gas stream and finally the plate was dried on a hotplate at 175 °C for ≥ 2 hours. After the drying phase, the plate was oxygen plasma treated (5 min, 200 W, 0.6 - 0.8 mbar, Diener Electonics PICO). The thickness of the planarization layer (SU-8 TF 6005) was targeted to 4 μm by using 3000 rpm spinning speed (SSE, OPTIcoat SST20+). The spinning speed for the pattern layer (SU-8 TF 6010) was also 3000 rpm. The UV-exposure was made with KARL SÜSS MA6/BA6 Mask-aligner, using i-Line filter. The exposed SU-8 layer was post-baked (4 min at 110 °C) and developed (3 min immersion + 30 s rinse with PGMEA) resulting in the structure height in average of 15,8 μm (15,4 - 16,2 μm, measured with a white light interferometer; Veeco, Wyko NT3000). All structures were positioned within a 40 mm radius from the centre to prevent edge bead problems and maintain structural homogeneity. Before the anti-adhesion treatment with Tridecafluoro-(1,1,2,2)-tetrahydrooctyl-trichlorosilane (F13-TCS) the plate was hard baked for 2 h in 230 °C and oxygen plasma treated (0.5 min, 200 W, 0.6 - 0.8 mbar). The anti-adhesion treatment process is described in more detail by Wang et al. [23] Finally, the plate was laser welded together with a blank nickel to form a sleeve with the exact measure for the imprinting cylinder (radius 65 mm, circumference 408 mm). Welding was purchased as a service from MK Fluidics Ltd (Finland). Blank nickel and welding seams were further treated with Teflon AF anti-adhesion coating as described previously. [16]

B. Silicone Deposition

A premixed two-component PDMS-based silicone elastomer (Wacker Elastosil RT-604, parts A+B in ratio of 9:1 by weight mixed with Hauschild Speedmixer DAC 330, 150 s, 2500 RPM, mixing done as separate step) was poured on to the running 100 mm wide web (i in Fig. 1 b) (Melinex ST506 125μm, corona treated) and leveled with a wire bar (ii in Fig. 1 b) (RK K-control coater bar with nominal wet thickness of 300 μm). Web speed in the coating was 0.2 m/min. The coating step is shown in Fig. 1b Silicone was deposited and leveled on the web with open doors under 1 atm of pressure, with a length of approximately 1.6 m for one trial. The eccentric mixer produces a nearly bubble free mixture and therefore a degassing step of the mixed silicone was omitted.

C. Microstructure Replication

R2R replication (iii in Fig 1 b) was executed at four different ambient pressures keeping other parameters as identical as possible. After coating a 1.6 m length of the web with mixed silicone, air evacuation was initiated for trials at reduced ambient pressure. Pressure was measured with Edwards P3 pressure gauge. Reaching 12.5 kPa pressure took 34 min 40 s and the same delay was kept in each trial between the PDMS coating and the replication, regardless of the ambient gas pressure. Imprint cylinder surface temperature in the beginning of imprinting in 1 atm was 127 - 129 °C, measured with a contact thermocouple from the surface. The web speed for the imprinting was 0.2 m/min. The web path around the imprint cylinder equals 167 mm of contact between running web and heated cylinder, leading to a contact time of 50 second with a web speed of 0.2 m/min. Both, infeed, and outfeed took place without a nip contact. Therefore, the imprint pressure was due to the imprint unit web tension (50 N). A 100 mm wide web was in contact over a length of 167 mm, resulting in a total contact area of 16700 mm^2. However, the pressure is not evenly distributed across the entire area, making it challenging to unambiguously define the exact imprint pressure.

The quality and extent of the curing process was examined with Attenuated Total Reflection Fourier Transform Infrared Spectroscopy (ATR FTIR, Bruker Alpha-P, with diamond crystal ATR). Mixed but non cured PDMS and oven cured PDMS was measured for reference purposes. FTIR spectra of reference and a R2R replicated sample are presented in **Fig. 2a**. With the only significant difference between spectra of different curing conditions being the peak at 912 cm^{-1}. It is attributed to of the Si-H group [33]. Si-H groups are used in the two-component RTV silicone rubbers for the crosslinking and curing by the platinum catalyzed addition reaction, more particularly a hydrosilylation reaction in this case [33]. The Si-H is consumed during the curing reaction and the decrease of Si-H concentration appears as a decreasing intensity of the IR signal along the reaction progress. The obtained spectra indicates that there are still Si-H groups present even in the oven cured reference sample after 30 min at 150 °C. Both the presented spectra are an average of 5 parallel spots measured (from the same sample set). The reference sample was chosen according to curing parameters that the material provider uses in the preparation of test samples for material specification measurements [34]. Furthermore, strength of the peaks in the spectra obtained from R2R produced samples indicate that there is significantly less Si-H present in the oven cured reference sample compared to R2R produced samples. It is, however not clear how much of the difference can be explained by the more complete crosslinking reaction or if the signal is decreased partly due to evaporation of the potential volatile hydrogen silane curing agent. On the other hand, in few hours after R2R replication, different web speeds (0.2; 0.5; 1.0 and 2.0 m/min) show different strength of the IR signal at 912 cm^{-1}(**Fig. 2b**) indicating more complete curing of PDMS with slower web speeds (slower web speed results in longer curing time). The length of the web path in contact with the hot cylinder was 167 mm and thus contact time of the silicone with the hot cylinder was 50 s, 20 s, 10 s and 5 s, respectively. PDMS is exposed to elevated temperature longer than the bare contact to the imprint cylinder due to heat capacity of the substrate and PDMS. Cooling to ambient temperature takes some time especially in the reduced ambient pressure. The outfeed roll and the following idle rolls inherently accelerate the web cooling due to thermal heat transfer (rolls warm during trial). We assume that the complete cooling time to reach room temperature is a matter of tens of seconds rather than minutes. After storing samples for eight weeks in 20 °C there is not any

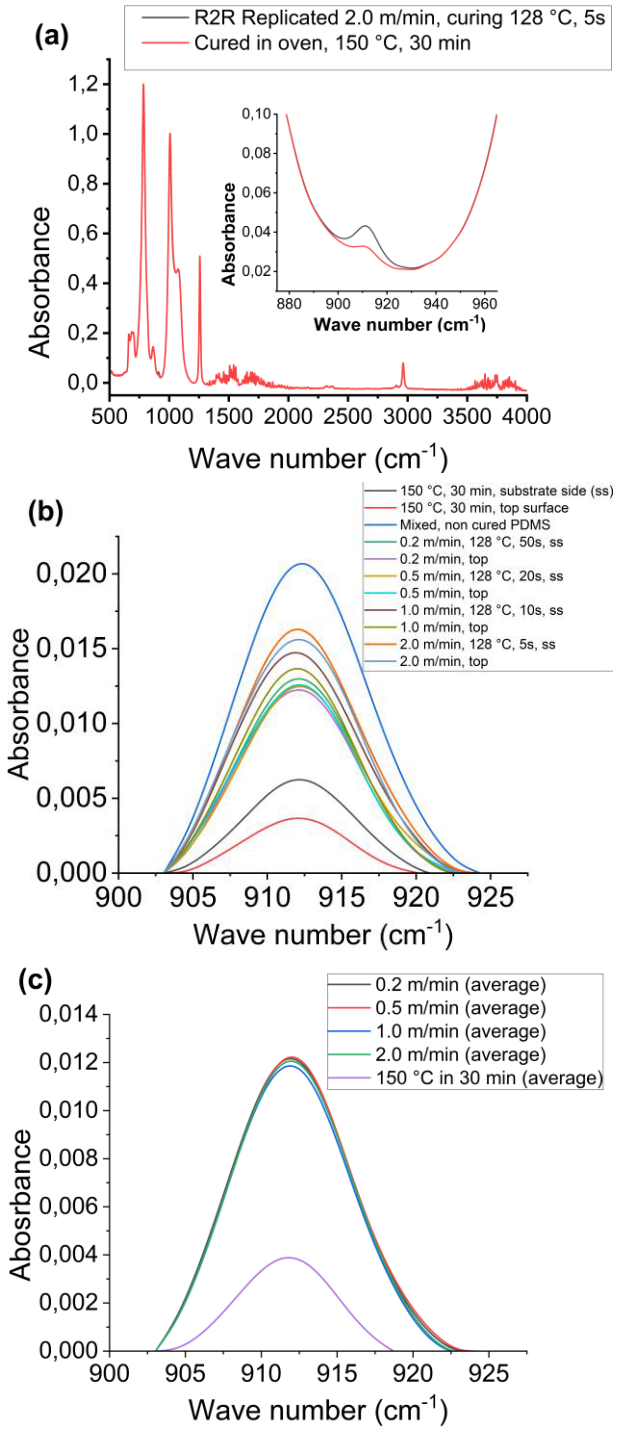

Fig. 2. (a) FTIR spectra of R2R replicated silicone and oven cured reference and a magnified view of 1000-800 cm^{-1}, (b) FTIR spectra of silicones replicated with different web speeds (different curing time) and oven cured reference and uncured silicone, (c) FTIR spectra of R2R replicated silicones after 8 weeks storage and oven cured reference.

more significant difference in IR signal at 912 cm^{-1} between different replication web speeds (**Fig. 2c**) despite the clear intensity variability immediately after the R2R imprinting.

III. Bubble Formation

A. Premixed Silicone Rheology

Rheology of the premixed, non-cured silicone is an important factor which affects how the formed bubbles can escape

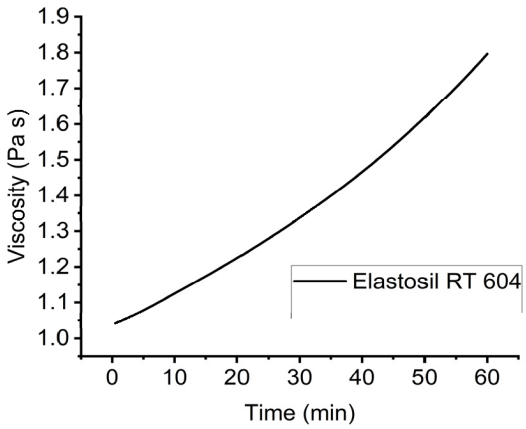

Fig. 3. Viscosity evolution of premixed Elastosil RT 604 PDMS in room temperature vs time.

the liquid silicone. Because curing reaction of the RTV silicones begin at room temperature immediately after mixing, we monitored viscosity of the uncured mixed silicone for 1 hour after mixing (mixed with Hauschild Speedmixer DAC 330, 150 s, 2500 RPM) to examine how much viscosity is changed between mixing and end of the replication. Start of replication took place at 34 min and end at < 42 min (three repeat á 0.4 m < 1.6 m each run). Viscosities were measured with Anton Paar MCR 302e rheometer using CP50-1TG measurement head. Measurement took place in 20 °C, pre-shear step 10 cm-1 for 30 s was used. Measurement step was 50 s-1 and viscosity was monitored for 60 min and recorded for every 30 s. Measured viscosities are presented in the **Fig. 3** Initial viscosity was 1.04 Pa s and after 60 min the viscosity was increased to 1.80 Pa s. Given mixed viscosity value is 800 m Pa s, measured according to ISO 3219 (component A: 1000 m Pa s and component B 200 m Pa s) [34]. This difference to the manufacturer's value can be attributed to various reasons; different measurement condition, mixing condition or different batch of materials, for example. Furthermore, the value by the manufacturer is given at 23 °C, we measured at 20 °C. According to the measurements, viscosity clearly increases in one hour which indicates that hydrosilylation reaction was started and ongoing. According to manufacturer, pot life of the material is 90 min (as up to 5000 m Pa s). Also, viscosity value shows that RT 604 silicone remains in the flowable range throughout the imprint run. Flowable viscosity range can be compared to, Dow Sylgard 184 and Momentive RTV-615, which are other commonly used silicone grades for micromolding. Their initial mixed viscosities were measured as 3.26 Pa s and 3.15 Pa s in the same conditions, increasing to 3.90 Pa s and 4.54 Pa s in one hour, respectively. Measured viscosity evolution graphs of Sylgard 184 and RTV-615 are presented in Supplementary material S2. All viscosities were measured at an ambient pressure of 1 atm. We assume that there would be no significant difference in viscosity behavior when imprinting is carried out at lower ambient pressures.

B. Optical Imaging and the Bubble Count

Rows of adjacent pillar structures, which is sensitive to bubble entrapment, were examined to compare the tendency of

TABLE I

ENTRAPPED GAS BUBBLES IN THE PILLAR STRUCTURES. SAME STRUCTURE IMPRINTED IN DIFFERENT AMBIENT PRESSURES

Ambient pressure	1 atm	½ atm	¼ atm	⅛ atm
Optical Image	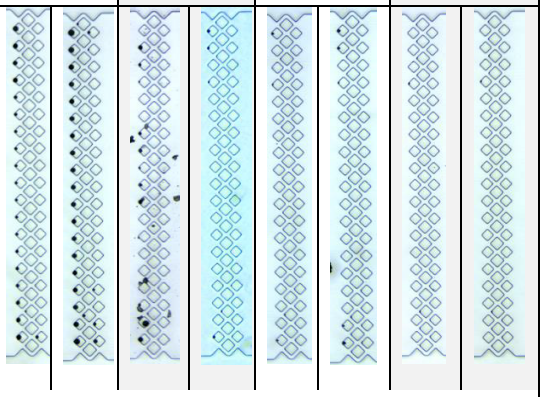			
Motion direction in replication event	Web path direction	Roll tool (mold) rotation direction		

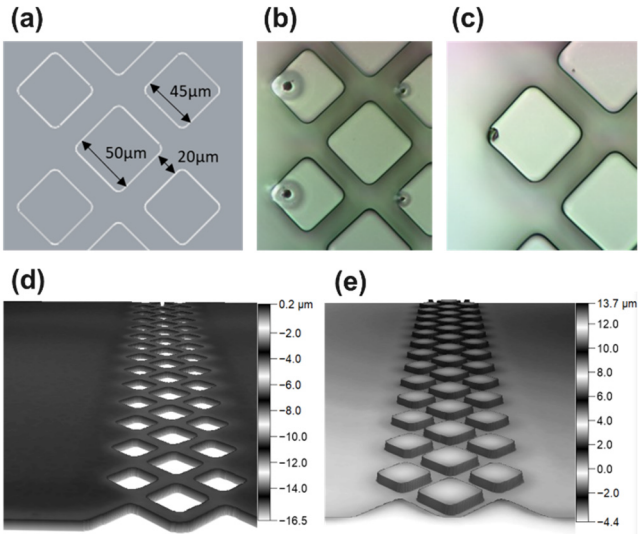

Fig. 4. (a) dimensions of the test patterns, (b) Optical image of typical bubbles in structures replicated in 1 atm, (c) One of the bubbles when replicated in 1/8 atm, (d) Interferometric image of the mold after trial, (e) Interferometric image of replicated silicone pillars.

bubble entrapment during imprinting at different ambient pressures. Additionally, this pillar matrix type is highly relevant for practical PDMS microfluidic applications, as similar pillar matrices are employed for particle separation [35]. Another implication for pillar matrixes is to increase active surface of the fluidic structures [36]. Replicated pillar structures were imaged with an optical microscope (Sensofar S Neox) to compare the amount and the size of the entrapped air bubbles. The imprint tool consisted of six identical parallel patterns, referred to as chips. Table I displays the second and third repetitions of chip 3 under different ambient pressures with further analysis and evidence found in the Supplementary material (**S3-S4**). The pillar pattern consisted of three rows of square shaped pillars with rounded corners. There were either 19 or 20 individual pillars in each row, middle row pillars were slightly larger in diameter than the pillars in two other rows (**Fig. 4a**). All images of each replicated pattern are presented in Supplementary material (**S5-S8**).

Total amount of pillars in each repetition was consequently 348. Although, some of the pillar patterns of the tool were stuck with silicone residue as seen in image in the Supplementary material (**S3**). After discluding these, there was 339 pillars in one repetition. We produced three repetitions in four different ambient pressures totaling 4068 individual pillars, which were optically imaged and visually examined each by each. Bubbles were categorized in to two groups (large or small bubble, examples shown in **S3**) and number of pillars with large and small bubbles or pillar without bubble were counted.

Percentage of the pillars with the bubbles out of all pillars are presented in the **Fig. 5.** In addition, there was a clear difference in the number of bubbles on the first, the second and the third pillar rows.

Images show that the bubbles are formed most often systematically in the third row in the sequence of the direction of web path (first row from the left in the images in **Table I**). Bubbles are most often formed systematically in the last end

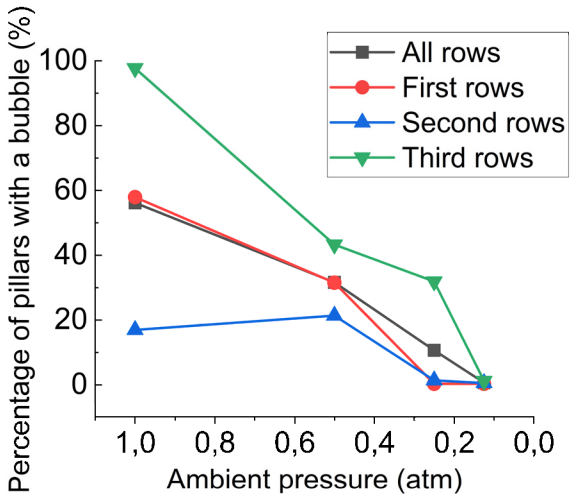

Fig. 5. Percentage of pillars with bubbles in different ambient pressures.

of the structure in the direction of the flow of the imprint resist. This is a consequence of the physical shape of the replicated structures, where gas can be entrapped and does not have a route to escape. Bubble sizes vary up to 30 μm in diameter. The pillar is 16 μm in height. If the largest bubbles are perfectly spherical their volumes correspond up to $\sim 1.4 \times 10^{-5}$mm^3 (pillar volume 3.2×10^{-5}mm^3) which is more than one third of the volume of the pillar. Due to residual silicone thickness, even such large bubble (diameter bigger than pillar height) can be spherical in shape. Fabrication at low ambient pressure resulted in significantly fewer large bubbles, with mostly only small bubbles remaining at ¼ and ⅛ atm. With the distribution of the bubbles in different pillar rows and in different pressures presented in the supplementary material (**S9**). In the last of the three pillar rows along the direction of imprinting (see **Fig. 5** and **Table I**), there was an air bubble in every individual pillar in all samples prepared at 1 atm pressure. Middle row comprised smaller bubbles in

average and total number of bubbled pillars was also lower compared to the first pillar row. Same tendency appeared in all tested ambient pressures. 1/8 atm showed the smallest bubbles in average size together with the smallest number of bubbles. There were still bubbles only in 0.7 % of all pillars (**Fig. 5**).

IV. Conclusion

In this work, we examined the effect of reduced ambient pressure on the bubble formation tendency in thermal R2R imprinting of microstructures with a PDMS based two component silicone elastomer. Also, we examined the completeness of silicone curing in the R2R replication process with the speeds of 0.2 – 2 m/min.

R2R replication at high speeds showed a probable incomplete curing, indicated by different IR signal strengths for the Si-H group at various web speeds. However, the difference in signal strength was negligible after 8 weeks, suggesting that post curing occurs, making higher web speeds viable for production as well.

This paper presents a method to reduce the amount of air bubble borne defects in R2R imprinted microstructures. We observed that reduction of the ambient pressure during the R2R replication results decreased number of bubble-type defects in the microstructures. This method may enable solutions to improve replication quality regardless of other process parameters or even material selection. A practical implication would be that processes and devices could be designed with a much higher level of freedom, as a vacuum would improve quality in most cases where bubble issues are faced. It is highly likely that the reduced ambient pressure method will also reduce air bubble defects in R2R UV-imprinting.

To our knowledge, this is the first publication describing roll-to-roll (R2R) imprinting performed in a partial vacuum. In the future, the influence of cavity shape, orientation, size and effect of nearby structures should be addressed to examine and validate the diversity of this process. In addition, future work should involve the use of UV-curable imprint resists as well.

Acknowledgment

Jenni Tomperi, Ulla Sarajärvi, and Pekka Ontero are acknowledged for R2R lines operation. Elina Hakola is acknowledged for assistance in rheology measurements and Dr. Sanna Aikio is acknowledged for CAD drawing. Prof. Caglar Elbuken and Seyedamirhosein Abdorahimzadeh from the University of Oulu are acknowledged for providing designs and CAD drawings of the pillar structures. The authors acknowledge Dr. Thomas M. Kraft for manuscript revision.

References

[1] S. Banik et al., "The revolution of PDMS microfluidics in cellular biology," *Crit. Rev. Biotechnol.*, vol. 43, no. 3, pp. 465–483, Apr. 2022, doi: 10.1080/07388551.2022.2034733.

[2] G. M. Whitesides and A. D. Stroock, "Flexible methods for microfluidics," *Phys. Today*, vol. 54, no. 6, pp. 42–48, Jun. 2001, doi: 10.1063/1.1387591.

[3] D. Qi, K. Zhang, G. Tian, B. Jiang, and Y. Huang, "Stretchable electronics based on PDMS substrates," *Adv. Mater.*, vol. 33, no. 6, Feb. 2021, Art. no. 2003155, doi: 10.1002/adma.202003155.

[4] G. Testa, G. Persichetti, and R. Bernini, "Planar optofluidic integration of ring resonator and microfluidic channels," *Micromachines*, vol. 13, no. 7, p. 1028, Jun. 2022, doi: 10.3390/mi13071028.

[5] I. E. Araci and S. R. Quake, "Microfluidic very large scale integration (mVLSI) with integrated micromechanical valves," *Lab Chip*, vol. 12, no. 16, p. 2803, 2012, doi: 10.1039/c2lc40258k.

[6] S. Bhattacharya, A. Datta, J. M. Berg, and S. Gangopadhyay, "Studies on surface wettability of poly(dimethyl) siloxane (PDMS) and glass under oxygen-plasma treatment and correlation with bond strength," *J. Microelectromech. Syst.*, vol. 14, no. 3, pp. 590–597, Jun. 2005, doi: 10.1109/JMEMS.2005.844746.

[7] M. Bélanger and Y. Marois, "Hemocompatibility, biocompatibility, inflammatory and in vivo studies of primary reference materials low-density polyethylene and polydimethylsiloxane: A review," *J. Biomed. Mater. Res.*, vol. 58, no. 5, pp. 467–477, Jan. 2001, doi: 10.1002/jbm.1043.

[8] C. M. Leung et al., "A guide to the organ-on-a-chip," *Nature Rev. Methods Primers*, vol. 2, no. 1, p. 33, May 2022, doi: 10.1038/s43586-022-00118-6.

[9] A. J. Thompson, L. J. Ma, T. J. Plegue, and J. A. Potkay, "Design analysis and optimization of a single-layer PDMS microfluidic artificial lung," *IEEE Trans. Biomed. Eng.*, vol. 66, no. 4, pp. 1082–1093, Apr. 2019, doi: 10.1109/TBME.2018.2866782.

[10] M. Bont, C. Barry, and S. Johnston, "A review of liquid silicone rubber injection molding: Process variables and process modeling," *Polym. Eng. Sci.*, vol. 61, no. 2, pp. 331–347, Feb. 2021, doi: 10.1002/pen.25618.

[11] H. Schift, "Nanoimprint lithography: An old story in modern times? A review," *J. Vac. Sci. Technol. B, Microelectron. Nanometer Struct. Process., Meas., Phenomena*, vol. 26, no. 2, pp. 458–480, Mar. 2008, doi: 10.1116/1.2890972.

[12] W. Qiao, W. Huang, Y. Liu, X. Li, L. Chen, and J. Tang, "Toward scalable flexible nanomanufacturing for photonic structures and devices," *Adv. Mater.*, vol. 28, no. 47, pp. 10353–10380, Dec. 2016, doi: 10.1002/adma.201601801.

[13] T. Mäkelä, T. Haatainen, P. Majander, J. Ahopelto, and V. Lambertini, "Continuous double-sided roll-to-roll imprinting of polymer film," *Jpn. J. Appl. Phys.*, vol. 47, no. 6, pp. 5142–5144, Jun. 2008, doi: 10.1143/jjap.47.5142.

[14] S. H. Ahn and L. J. Guo, "High-speed roll-to-roll nanoimprint lithography on flexible plastic substrates," *Adv. Mater.*, vol. 20, no. 11, pp. 2044–2049, Jun. 2008, doi: 10.1002/adma.200702650.

[15] E. K. Sackmann, A. L. Fulton, and D. J. Beebe, "The present and future role of microfluidics in biomedical research," *Nature*, vol. 507, no. 7491, pp. 181–189, Mar. 2014, doi: 10.1038/nature13118.

[16] J. Hiltunen et al., "Roll-to-roll fabrication of integrated PDMS–paper microfluidics for nucleic acid amplification," *Lab a Chip*, vol. 18, no. 11, pp. 1552–1559, May 2018, doi: 10.1039/c8lc00269j.

[17] O. H. Huttunen et al., "Roll-to-roll screen-printed silver conductors on a polydimethyl siloxane substrate for stretchable electronics," *Ind. Eng. Chem. Res.*, vol. 58, no. 43, pp. 19909–19916, Oct. 2019, doi: 10.1021/ACS.IECR.9B03628.

[18] O. Huttunen, M. H. Behfar, J. Hiitola-Keinänen, and J. Hiltunen, "Electronic tattoo with transferable printed electrodes and interconnects for wireless electrophysiology monitoring," *Adv. Mater. Technol.*, vol. 7, no. 8, Aug. 2022, Art. no. 2101496, doi: 10.1002/admt.202101496.

[19] X. Li et al., "Scalable fabrication of carbon materials based silicon rubber for highly stretchable e-textile sensor," *Nanotechnol. Rev.*, vol. 9, no. 1, pp. 1183–1191, Dec. 2020, doi: 10.1515/ntrev-2020-0088.

[20] K. Gao, H. Shen, Y. Liu, Q. Zhao, Y. Li, and J. Liu, "Random inverted pyramid textured polydimethylsiloxane radiative cooling emitter for the heat dissipation of silicon solar cells," *Sol. Energy*, vol. 236, pp. 703–711, Apr. 2022, doi: 10.1016/j.solener.2022.03.040.

[21] X. Song, X. C. Shan, S. L. Chow, X. Y. Deng, and W. S. Teo, "Numerical and experimental study of the filling stage of roll-to-roll UV embossing process with micro features," *Microsyst. Technol.*, vol. 21, no. 8, pp. 1729–1738, Aug. 2015, doi: 10.1007/s00542-014-2290-9.

[22] H. Ye, L. Shen, M. Li, and Q. Zhang, "Bubble defect control in low-cost roll-to-roll ultraviolet imprint lithography," *Micro Nano Lett.*, vol. 9, no. 1, pp. 28–30, Jan. 2014, doi: 10.1049/mnl.2013.0618.

[23] L. Peng, H. Wu, P. Yi, and X. Lai, "Study on bubble defects in roll-to-roll UV imprinting process for micropyramid arrays II: Numerical study," *J. Vac. Sci. Technol. B, Nanotechnol. Microelectron., Mater., Process., Meas., Phenomena*, vol. 34, no. 5, Aug. 2016, Art. no. 051203, doi: 10.1116/1.4960693.

[24] H. Wu, P. Yi, L. Peng, and X. Lai, "Study on bubble defects in roll-to-roll UV imprinting process for micropyramid arrays. I. Experiments," *J. Vac. Sci. Technol. B, Nanotechnol. Microelectron., Mater., Process., Meas., Phenomena*, vol. 34, no. 2, Feb. 2016, Art. no. 021201, doi: 10.1116/1.4941445.

[25] H. C. Ye, L.-G. Shen, B. Tao, and M.-J. Li, "A study of the bubbles in UV micro roll-to-roll imprinting," *Int. Polym. Process.*, vol. 29, no. 5, pp. 602–606, Nov. 2014, doi: 10.3139/217.2911.

[26] A. Fuchs, M. Bender, U. Plachetka, U. Hermanns, and H. Kurz, "Ultraviolet-based nanoimprint at reduced environmental pressure," *J. Vac. Sci. Technol. B, Microelectron. Nanometer Struct. Process., Meas., Phenomena*, vol. 23, no. 6, pp. 2925–2928, Nov. 2005, doi: 10.1116/1.2132325.

[27] S. Matsui, H. Hiroshima, Y. Hirai, and M. Nakagawa, "Innovative UV nanoimprint lithography using a condensable alternative chlorofluorocarbon atmosphere," *Microelectronic Eng.*, vol. 133, pp. 134–155, Feb. 2015, doi: 10.1016/j.mee.2014.10.016.

[28] R. Kirchner, L. Nüske, A. Finn, B. Lu, and W.-J. Fischer, "Stamp-and-repeat UV-imprinting of spin-coated films: Pre-exposure and imprint defects," *Microelectronic Eng.*, vol. 97, pp. 117–121, Sep. 2012, doi: 10.1016/j.mee.2012.03.037.

[29] H.-C. Scheer, M. Papenheim, K. Dhima, S. Wang, and C. Steinberg, "Aspects of cavity filling with nano imprint," *Microsyst. Technol.*, vol. 21, no. 8, pp. 1595–1605, Aug. 2015, doi: 10.1007/s00542-014-2376-4.

[30] X. Liang, H. Tan, Z. Fu, and S. Y. Chou, "Air bubble formation and dissolution in dispensing nanoimprint lithography," *Nanotechnology*, vol. 18, no. 2, Jan. 2007, Art. no. 025303, doi: 10.1088/0957-4484/18/2/025303.

[31] C. Yang, M. Li, J. Wang, H. Ye, and J. Qiu, "Residual layer assisted demolding in roll-to-roll UV imprint lithography," *Microelectronic Eng.*, vol. 217, Sep. 2019, Art. no. 111110, doi: 10.1016/j.mee.2019.111110.

[32] W. Xu, P. Yi, J. Gao, Y. Deng, L. Peng, and X. Lai, "Large-area stable superhydrophobic poly(dimethylsiloxane) films fabricated by thermal curing via a chemically etched template," *ACS Appl. Mater. Interfaces*, vol. 12, no. 2, pp. 3042–3050, Jan. 2020, doi: 10.1021/acsami.9b19677.

[33] D. Cai, A. Neyer, R. Kuckuk, and H. M. Heise, "Raman, mid-infrared, near-infrared and ultraviolet–visible spectroscopy of PDMS silicone rubber for characterization of polymer optical waveguide materials," *J. Mol. Struct.*, vol. 976, nos. 1–3, pp. 274–281, Jul. 2010, doi: 10.1016/j.molstruc.2010.03.054.

[34] *WACKER ELASTOSIL RT 604 A/B Technical Datasheet by the Material Manufacturer*. Accessed: Dec. 13, 2022. [Online]. Available: https://www.wacker.com/h/en-us/medias/ELASTOSIL-RT-604-AB-en-2020.07.01.pdf

[35] M. Bayareh, "An updated review on particle separation in passive microfluidic devices," *Chem. Eng. Process. Process Intensification*, vol. 153, Jul. 2020, Art. no. 107984, doi: 10.1016/j.cep.2020.107984.

[36] S. Feola et al., "PeptiCHIP: A microfluidic platform for tumor antigen landscape identification," *ACS Nano*, vol. 15, no. 10, pp. 15992–16010, Oct. 2021, doi: 10.1021/acsnano.1c04371.